Tuning Frictional Properties of Kirigami Altered Graphene Sheets using Molecular Dynamics and Machine Learning

Designing a Negative Friction Coefficient

Mikkel Metzsch Jensen

Thesis submitted for the degree of
Master in Computational Science: Materials Science
60 credits

Department of Physics
Faculty of mathematics and natural sciences

UNIVERSITY OF OSLO

Spring 2023

Tuning Frictional Properties of Kirigami Altered Graphene Sheets using Molecular Dynamics and Machine Learning

Designing a Negative Friction Coefficient

Mikkel Metzsch Jensen

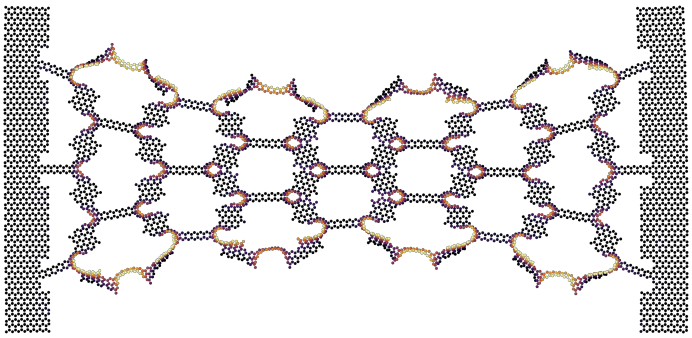

Tuning Frictional Properties of Kirigami Altered Graphene Sheets using Molecular Dynamics and Machine Learning

http://www.duo.uio.no/

Printed: Reprosentralen, University of Oslo

Abstract

Abstract.

Acknowledgments

Acknowledgments.

List of Symbols

F_N Normal force (normal load)

Acronyms

MD Molecular Dynamics. 2, 3, 9, 10, 12

ML Machine Learning. 2, 3, 10

Contents

Chapter 1

Introduction

Structure of Motivation section:

1. Introduce and motivate friction broadly.
2. Motives for friction control using a grasping robot as example.
3. Analog to gecko feet where adhesive properties are turned on and off.
4. Interest in origin of friction through nanoscale studies which further motivates the use of MD.
5. Intro to metamaterials and the use of kirigami designs,
6. How to optimize kirigami designs with reference to Hanakata and motivating the use of ML.
7. Out-of-plane buckling motivates the use of kirigami for frictional properties.

Does some of the latter paragraphs belong to the approach section?

1.1 Motivation

Friction is a fundamental force that takes part in most of all interactions with physical matter. Even though the everyday person might not be familiar with the term *friction* we recognize it as the inherent resistance to sliding motion. Some surfaces appear slippery and some rough, and we know intuitively that sliding down a snow covered hill is much more exciting than its grassy counterpart. Without friction, it would not be possible to walk across a flat surface, lean against the wall without falling over or secure an object by the use of nails or screws [p. 5] [1]. It is probably safe to say that the concept of friction is integrated in our everyday life to such an extent that most people take it for granted. However, the efforts to control friction dates back to the early civilization (3500 B.C.) with the use of the wheel and lubricants to reduce friction in translational motion [2]. Today, friction is considered a part of the wider field *tribology* derived from the Greek word *Tribos* meaning "rubbing" and includes the science of friction, wear and lubrication [2]. The most compelling motivation to study tribology is ultimately to gain full control of friction and wear for various technical applications. Especially, reducing friction is of great interest as this has tremendous advantages for energy effeciency. It has been reported that tribological problems have a significant potential for economic and environmental improvements [3]:

> "On global scale, these savings would amount to 1.4% of the GDP annually and 8.7% of the total energy consumption in the long term." [4].

On the other hand, the reduction of friction is not the only sensible application for tribological studies. Controlling frictional properties, besides minimization, might be of interest in the development of a grasping robot where a finetuned object handling is required. While achieving a certain "constant" friction response is readily obtained through appropiate material choices during manufacturing, we are yet to unlock the capabilities to alter friction dynamically on the go. One example from nature inspiring us to think along theese lines are the gecko feet. More precisely, the Tokay gecko has recieved a lot of attention in scientific studies aiming to unravel the underlying

mechanism of its "togglable" adhesion properties. Although geckos are able to produce large adhesive forces, they retain the ability to remove their feet from an attachment surface at will [5]. This makes the gecko able to achieve a high adhesion on the feet when climbing a vertical surface while lifting it for the next step remains reletively effortless. For a grasping robot we might consider an analog frictional concept of a surface material that can change from slippery to rough on demand depending on specific tasks.

In the recent years an increasing amount of interest has gone into the studies of the microscopic origin of friction, due to the increased possibilities in surface preperation and the development of nanoscale experimental methods. Nano-friction is also of great concern for the field of nano-machining where the frictional properties between the tool and the workpiece dictates machining charascteristics [3]. With concurrent progress in computational power and devolopment of Molecular Dynamics (MD), numerical investigations serve as an extremely useful tool for getting insight into the nanoscale mechanics associated with friction. This simulation based approach can be considered as a "numerical experiment" enabling us to create and probe a variety of high complexity systems which are still out of reach for modern experimental methods.

In materials science such MD-based numerical studies have been used to explore the concept of so-called *metamaterials* where material compositions are designed meticulously to enhance certain physical properties [6][7][8][9][10][11]. This is often achieved either by intertwining different material types or removing certain regions completely. In recent papers by Hanakata et al. [6](2018) [7](2020) numerical studies have showcased that mechanical properties of a graphene sheet, in this case yield stress and yield strain, can be altered through the introduction of so-called *kirigami* inspired cuts into the sheet. Kirigami is a variation of origami where the paper is cut additionally to being folded. While these methods originate as an art form, aiming to produce various artistic objects, they have proven to be applicable in a wide range of fields such as optics, physics, biology, chemistry and engineering [12]. Various forms of stimuli enable direct 2D to 3D transformations through folding, bending, and twisting of microstructures. While orginal human designs have contributed to specific scientiffic applications in the past, the future of this field is highly driven by the question of how to generate new designs optimized for certain physical properties. However, the complexity of such systems and the associated design space makes for seemingly intractable problems ruling out analytic solutions.

Earlier architecture design approaches such as bioinspiration, looking at gecko feet for instance, and Edisonian, based on trial and error, generally rely on prioir knowdelegde and an experienced designer [9]. While the Edisonian approach is certainly more feasible through numerical studies than real world experiments, the number of combinations in the design space rather quickly becomes too large for a systematic search, even when considering the simulation time on modern day hardware. However, this computational time constraint can be relaxed by the use of machine learning (ML) which have proven successful in the establishment of a mapping from the design space to physical properties of interest. This gives rise to two new styles of design approaches: One, by utilizing the prediction from a trained network we can skip the MD simulations all together resulting in an *accelerated search* of designs. This can be further improved by guiding the search accordingly to the most promising candidates, as for instance done with the *genetic algorithm* which suggest new designs based on mutation and crossing of the best candidates so far. Another, even more sophisticated approach, is through generative methods such as *Generative Adversarial Networks* (GAN). By working with a so-called *encoder-decoder* network structure, one can build a model that reverses the prediction process. That is, the model predicts a design from a set of physical target properties. In the papers by Hanakata et al. both the *accelerated search* and the *inverse design* approach was proven successful to create novel metamaterial kirigami designs with the graphene sheet.

Hanakata et al. attributes the variety in yield properties to the non-linear effects arrising from the out-of-plane buckling of the sheet. Since it is generally accepted that the surface roughness is of great importance for frictional properties it can be hypothesized that the kirigami cut and stretch procedure can also be exploited for the design of frictional metamaterials. For certain designs we might hope to find a relationship between stretching of the sheet and frictional properties. If signifciant, this could give rise to a variability of the friction reponse beyond manufacturing material choice. For instance, the grasping robot might apply such a material as artifical skin for which stretching or relaxing of the surface could result in a changeable friction strength; Slippery and smooth when in contact with people and rough and firmly gripping when moving heavy objects. In addition, a possible coupling between stretch and the normal load through a nanomachine design would allow for an altered friction coefficient. This invites the idea of non-linear friction coeffcients which might in theory also take on negative values given the right response from stretching. The latter would constitute an extremely rare property. This has (only?) been reported indirectly for bulk graphite by Deng et al. [13] where the friction kept increasing during the unloading phase. Check for other cases and what I can really say here.

To the best of our knowledge, kirigami has not yet been implemented to alter the frictional properties of a nanoscale system. In a recent paper by Liefferink et al. [14](2021) it is reported that macroscale kirigami can be used to dynamically control the macroscale roughness of a surface through stretching which was used to change the frictional coeffcient by more than one order of magnitude. This support the idea that kirigami designs can in fact be used to alter friction, but we believe that taking this concept to the nanoscale regime would envolve a different set of underlying mechanisms and thus contribute to new insight in this field.

1.2 Goals

In this thesis we investigate the possibility to alter and control the frictional properties of a graphene sheet through application of kirigami inspired cuts and stretching of the sheet. With the use of MD simulations we evaluate the friction properties under different physical conditions in order to get insight into the prospects of this field. By evaluating variations of two kirigami inspired patterns and a series of random walk generated patterns we create a dataset containing information of the frictional properties associated with each design under different load and stretch conditions. We apply ML to the dataset and use an accelerated search approach to optimize for different properties of interest. The subtask of the thesis are presented more comprehensively in the following.

1. Define a sheet indexing that allows for an unqiue mapping of patterns between a hexagonal graphene lattice representation to a matrix representation suited for numerical analysis.
2. Design a MD simulation procedure to evaluate the frictional properties of a given graphene sheet under specified physical conditions such as load, stretch, temperature etc.
3. Find and implement suitable kirigami patterns which exhibit out-of-plane buckling under tensile load. This includes the creation of a framework for creating variations within each pattern class. Additionally create a procedure for generating different styles of random walk patterns.
4. Perform a pilot study of a representative subset of patterns in order to determine appropriate simulation parameters to use for the further study along with an analysis of the frictional properties shown in the subset.
5. Create a dataset consisting of the chosen kirigami variations and random walk patterns and analyse data trends.
6. Train a neural network to map from the design space to physical properties such as mean friction, maximum friction, contact area etc. and evaluate the performance.
7. Perform an accelerated search optimizing for interesting frictional properties using the ML model. This should be done both through the pattern generation procedures and by following a genetic algorithm approach.
8. Use the most promising candidtes from the accelerated search to investigate the prospects of creating a nanomachine setup which exhibits a negative friction coefficient.
9. Study certain designs of interest with the scope of revealing underling mechanism. This includes simple correlation analysis but also a visualization of feature and gradient maps of the ML network.

Is the list of subtask to specific? Some of the details here might be better suited for the thesis structure section.

1.3 Contributions

What did I actually achieve

1.4 Thesis structure

How is the thesis structured.

Part I

Background Theory

Part II

Simulations

Chapter 2

Pilot study

Having defined our system, we carry out an initial study of the numerical approach. This includes an analysis of how to define and measure the frictional properties of interest, and an investigation of the main parameters governing the numerical solutions. From this point of view we decide on a suitable set of parameters for the remaining study. Additionally, we investigate the frictional behaviour under the variation of load and stretch for a selected set of configurations which serves as a baseline for later comparison.

2.1 Friction simulation parameters

The MD simulation is governed by a small set of parameters, some which are related directly to the numerical aspects of the simulation and other to the physical conditions in the simmulation. Thus, we differentiate between the two main categories: 1) *Physical*, parameters which alter the physical conditions of the "numerical experiment" and are expected to effect the frictional behaviour. 2) *Numerical*, parameters which are related more closely to the numerical procedure itself, expected to influence the simulation dynamics, which should be chosen to ensure the most stable results. For the purpose of creating the machine learning dataset most of these parameters will be kept constant with only a subset of the physical parameters being varied. The parameters are summarized in Table 2.1 with the grey shaded area denoting the parameters which we will vary for the dataset. Due to the great number of parameters it is unreasonable to make an exhaustive search of all parameters, in order to choose the final settings. Instead, we take a basis in the parameters used in similar studies SOURCES and adjust them as we carry out the analysis of the simulation results. Thus, we start at values most representative for other similar simulations and adjust according to the stability of the results and the computation time. Since we are going to introduce a lot of complexity to the system, through the cut and stretch deformation, we are less strict about meeting other paramter criterias (does this make sense). The final parameter choice is shown in Table 2.1 which we be the default values in the following study, i.e. when nothing is stated explicitly we will use these parameters. As we analyse the data we will provide further arguments for specific choices made.

Table 2.1: Parameters of the numerical MD simulation for measuring friction. The values correspond to the final choice used for the dataset. The shaded area denote the parameters varied in the ML dataset.

Category	Parameter	Value	Description
Physical	T	300 K	Temperature.
	v_{slide}	20 m/s	Sliding speed for the sheet translation.
	K	inf	Spring constant for the coupling between the virtuel atom and the sheet pull blocks.
	Scan direction	$(x, y) = (0, 1)$ (zigzag direction)	The direction for which we translate the sheet.
	Sheet configuration	Contiguous	Binary mapping describing which atoms are removed (0) and which is still present (1) in the graphene sheet.
	Stretch amount	0% - rupture	The relative stretch of the sheet.
	F_N	[0.1, 10] nN	Applied normal force to the pull blocks.
Numerical	dt	1 fs	Integration timestep.
	t_R	15 ps	Relaxtion time before strething.
	Pauses	5 ps	Relaxtion pauses after stretch, and during the normal load phase (before translating the sheet).
	Stretch Speed	0.01 ps^{-1}	The rate of stretching for the sheet.
	Slide distance	400 Å	How far to translate the sheet.
	Sheet size	130.029×163.219 Å	Spatial 2D size of the sheet.
	Pull block size	$2 \times 130.029 \times 15.183$ Å	Spatial 2D size of the pull blocks.

2.2 Force traces

We begin by assessing the force traces for a single friction simulation using the default parameters shown in **??** for a non-cut sheet with no stretch applied and a normal force of 1 nN.

2.2.1 Force oscillations

We evaluate the friction force as the force acting on the sheet from the substrate. We consider initially the force componenet $F_{\parallel}$ parallel to the drag direction as plotted in Fig. 2.1. The sample rate is 10 ps^{-1} = 100 timesteps^{-1} for which each sample is the mean value of the preceding 100 timesteps. We observe immediately that the data carriers oscillations on different time scales which matches our expectations for sliding on periodic surfaces. By applying a savgol filter to the data with a polyorder of 5 and window length of 150 timesteps, corresponding to a sliding distance of 3 Å or a time window of 15 ps, we can qualitatively point out at least two different frequencies of osccilation. During the first 10 Å of sliding in Fig. 2.1a we see roughly three waves on the savgol filter corresponding to a relative high frequency, while on the scale of 100 Å of sliding in Fig. 2.1b the same savgol filter reveals a lower frequency on top, creating the visual pattern of a wavepacket. The data does not indicate clear signs of stick-slip behaviour as otherwise found in other studies, e.g. by Zhu and Li [15] for graphene on gold, who saw a more typical saw tooth shape in the force trace. submitted run to ensure that we match Zhu and Li's condition. However, if they look like the ones for K = 30 N/m and 1 m/s we do not see the stick-slip behaviour really.

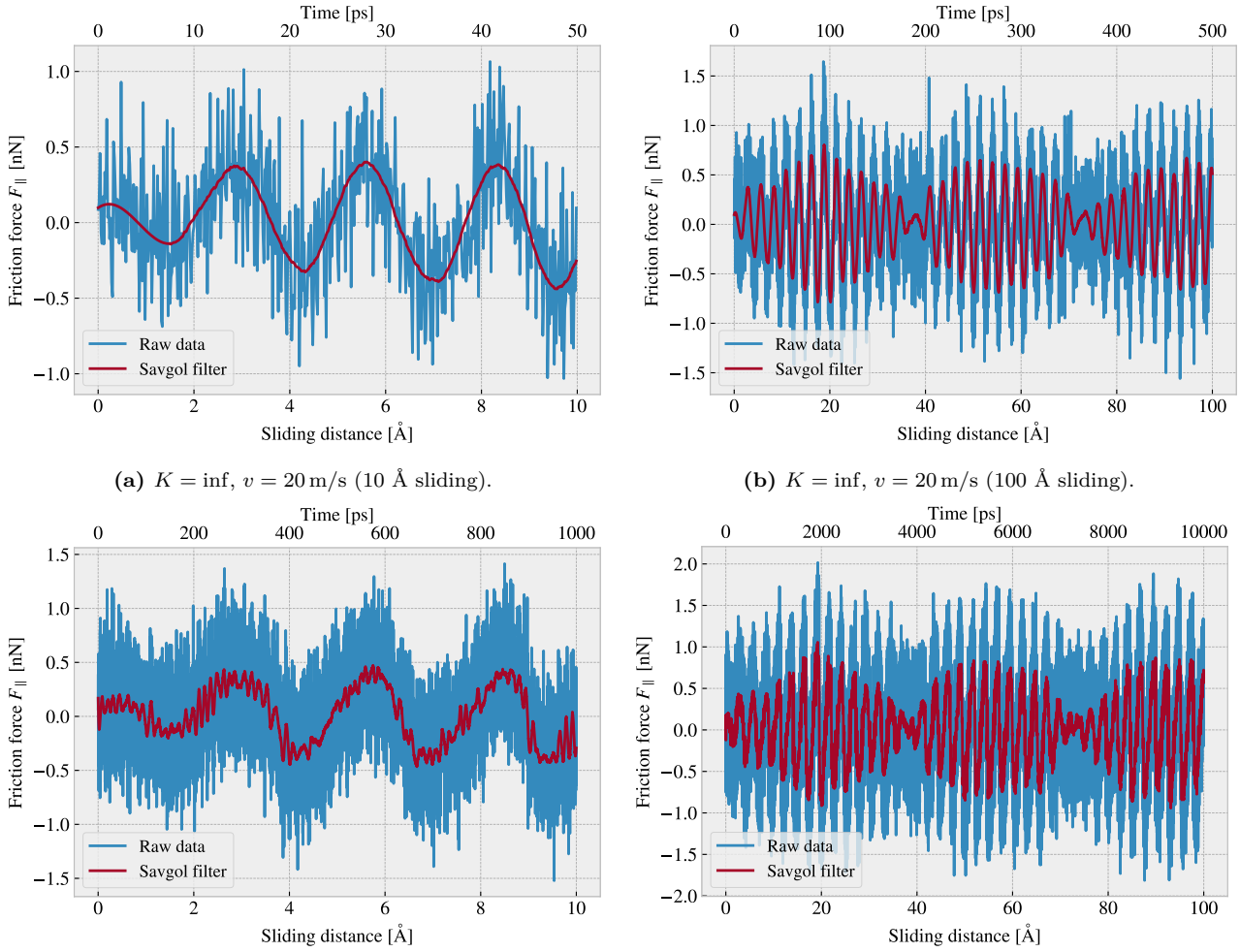

(a) $K = \inf$, $v = 20\,\mathrm{m/s}$ (10 Å sliding).

(b) $K = \inf$, $v = 20\,\mathrm{m/s}$ (100 Å sliding).

(c) $K = 30\,\mathrm{N/m}$, $v = 1\,\mathrm{m/s}$ (10 Å sliding).

(d) $K = 30\,\mathrm{N/m}$, $v = 1\,\mathrm{m/s}$ (100 Å sliding).

Figure 2.1: Friction force $F_{\parallel}$ with respect to the drag direction between (full) sheet and substrate versus sliding distance. The sliding distance is measured by the constant movement of the virtual atom and not the COM of the sheet. However, we expect these measures to be fairly identical due the fact that the pull blocks is rigidly coupled to the virtual atom. The red line represents a savgol filter with window polyorder 5 and window length of 150 timesteps (corresponding to a sliding distance of 3 Å or a time window of 15 ps).

By performing a Fourier Transform on the data (default parameters) we can quantify the leading frequencies observed in figure Fig. 2.1a and Fig. 2.1b. The Fourier transform is shown in Fig. 2.2a, and by plotting the two most dominant frequencies $f_1 = 0.0074\ \mathrm{ps}^{-1}$ and $f_2 = 0.0079\ \mathrm{ps}^{-1}$ as $\sin(2\pi f_1) + \sin(2\pi f_2)$ we find a qualitatively convincing fit to the observed wavepacket shape as seen in Fig. 2.2b. By using the trigonometric identity

$$\begin{aligned}\sin(a+b) &= \sin(a)\cos(b) + \cos(a)\sin(b),\\ \sin(a-b) &= \sin(a)\cos(b) - \cos(a)\sin(b),\end{aligned}$$

and decomposing the frequencies as $f_1 = a - b$, $f_2 = a + b$, we can rewrite the sine sum as the sinusoidal product

$$\begin{aligned}\sin(2\pi f_1) + \sin(2\pi f_2) &= \sin\big(2\pi(a-b)\big) + \sin\big(2\pi(a+b)\big)\\ &= \sin(2\pi a)\cos(2\pi b) + \cancel{\cos(2\pi a)\sin(2\pi b)} + \sin(2\pi a)\cos(2\pi b) - \cancel{\cos(2\pi a)\sin(2\pi b)}\\ &= 2\sin(2\pi a)\cos(2\pi b),\end{aligned}$$

with

$$a = \frac{f_1 + f_2}{2} = 0.0763 \pm 0.0005\,\mathrm{ps}^{-1}, \qquad b = \frac{f_2 - f_1}{2} = 0.0028 \pm 0.0005\,\mathrm{ps}^{-1},$$
$$= 0.381 \pm 0.003\,\mathrm{Å}^{-1}, \qquad = 0.014 \pm 0.003\,\mathrm{Å}^{-1},$$

where the latter frequency is denoted with respect to the sliding distance. This makes us recognize the high osccilation frequency as a and the low frequency as b. The faster one has a period of $T_a = 2.62 \pm 0.02$ Å[1]. This corresponds well with the magnitude of the lattice spacing and especialy that of graphene at 2.46 Å as expected theoretically. The longer period $T_b = 71 \pm 15$ Å^{-1} is not obviously explained. The build up in friction force is reminiscent of a friction strengthening, but the periodic oscillation does not really support this idea. Instead, we might attribute it to some kind of phonon resosnance which could be a physical phenonama or simply a feature of our MD modelling.

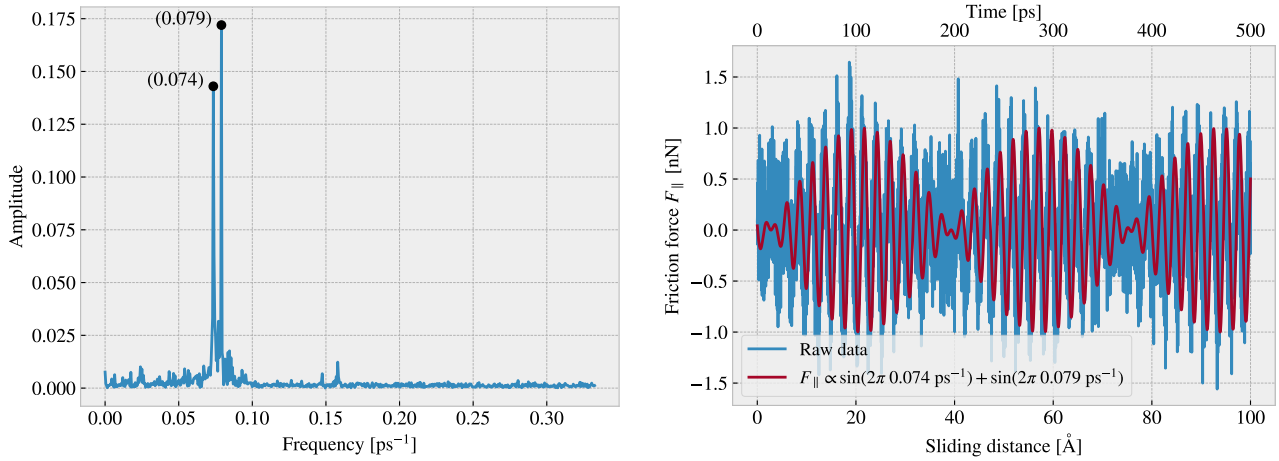

(a) FT result shown for a reduced frequency range.

(b) Two most dominant frequencies applied to the data from Fig. 2.1b

Figure 2.2: Fourier transform analysis of the full friction force data (all 400 Å sliding distance) shown in Fig. 2.1. (a) shows the two most dominant frequency peaks. Note that no significant peaks was found in a higher frequency than included here. (b) shows a comparison between the raw data and the wavefunction corresponding to the two peaks in figure (a).

2.2.2 Decompositions

In the previous analysis we have looked only at the friction force for the full sheet, including the rigid pull blocks, and with respect to the drag direction. We found this way of measuring the friction force to be the most reliable, but we will present the underlying arguments for this choice in the following.

Due to the fact that we are only applying cuts to the inner sheet, and not the pull blocks, it might seem more natural to only consider the friction on that part. If the desired frictional properties can be achieved by altering the inner sheet one can argue that any opposing effects from the pull blocks can be mitigated by scaling the relative size between the inner sheet and the pull blocks. However, when looking at the force traces decomposed with respect to the inner sheet and pull block regions respectivly (see Fig. 2.3a), we observe that the friction force arrising from those parts are seemingly antisymmetric. That is, the distribution of the fricitonal pull from the substrate on the sheet is oscillating between the inner sheet and the pull block. Keeping in mind that normal force is only applied to the pull blocks we might take this as an integrated feature of the system which does not nessecary dissapear when changing the spatial ratio between inner sheet and pull block. Any interesting friciton properties might depend on this internal distribution of forces. Hence, we hedge our bets and use the full sheet friction force as a hollistic approach to avoid excluding relevant data in the measurements.

Similar we might question the decision of only considering the frictional force projected onto the sliding direction as we are then neglecting the "side shift" induced during the slide phase. In Fig. 2.3b we see the

[1]The uncertainty Δy is calculated as $\Delta y = \left|\frac{\partial y}{\partial x}\Delta x\right|$ for uncertainty Δx and $y(x)$

decomposition in terms of force components parallel $F_{\parallel}$ and perpendicular $F_{\perp}$ to the sliding direction respectively. We notice that the most dominant trend appears for the parallel component. If we want to include the perpendicular component as well we would have to evaluate friction as the length of the force vector instead. This would remove the sign of the force direction and skew the whole friction force above as we clearly see both negative and positive contributions in the force trace. One option to accommodate this issue is by using the vector length for the magnitude but keeping the sign from the parallel component. However, we omit such compromises as this might make the measurement interpretation unessercary complex, and we use only the parallel component going forward.

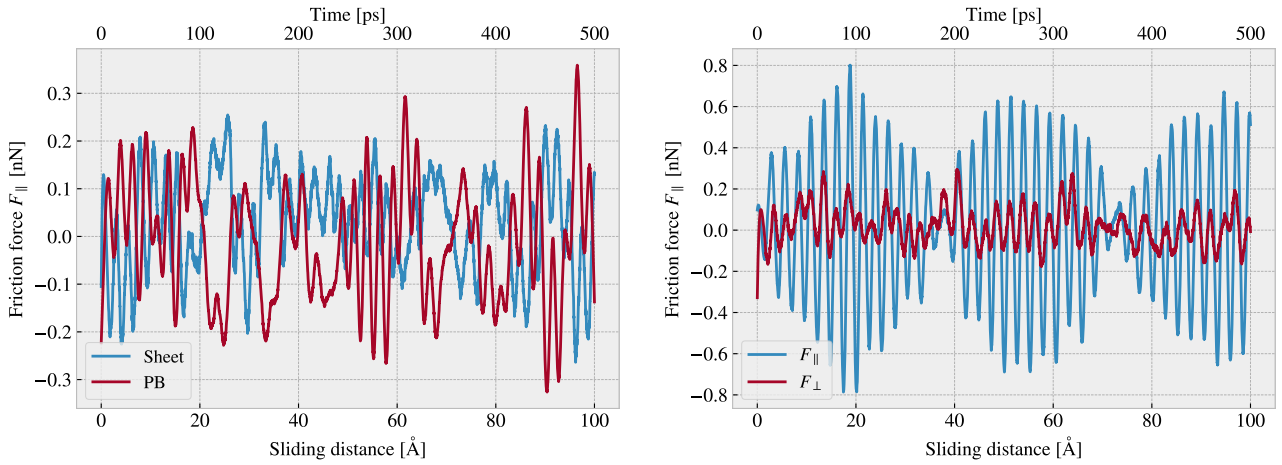

(a) Decomposition into group inner sheet (sheet) and pull blocks (PB).

(b) Decomposition into parallel ($F_{\parallel}$) and perpendicular ($F_{\perp}$) to drag sliding direction.

Figure 2.3: Friction force decomposition on the data shown in Fig. 2.1 with applied savgol filters similar to that of Fig. 2.1b with window polyorder 5 and window length of 150 timesteps (corresponding to a sliding distance of 3 Å or a time window of 15 ps).

2.2.3 Center of mass path

Go through here again when done with the stick-slip motion analysis.

From the previous observations of the friction force time series we see evidence of a stick-slip behvaiour. Specially, we see in Fig. 2.3b that this might be the case both parallel and perpendicular to the sliding direction. By looking at the x, y-position for the sheet center of mass (COM) change to CM we observe the stick-slip motion manifested as a variation in COM speed combinned with a side to side motion as shown in figure $Fig.$ 2.4a. In an attempt to increase the magnitude of the slips we evaluate a similar simulation with spring contant $K = 30\,\mathrm{N/m}$ (see figure Fig. 2.4b) in contrast to that of an infinte spring constant. While the maximum slip speed stays within a similar order of magnitude the slip length in the sliding direction is increased along with the side to side motion. Note that the axis scale is different between Fig. 2.4a and Fig. 2.4a. However, in both cases we observe that the side to side motion is associated with a low speed, meaning that is more reminiscent of a "slow" creep alignment with the substrate than a slip.

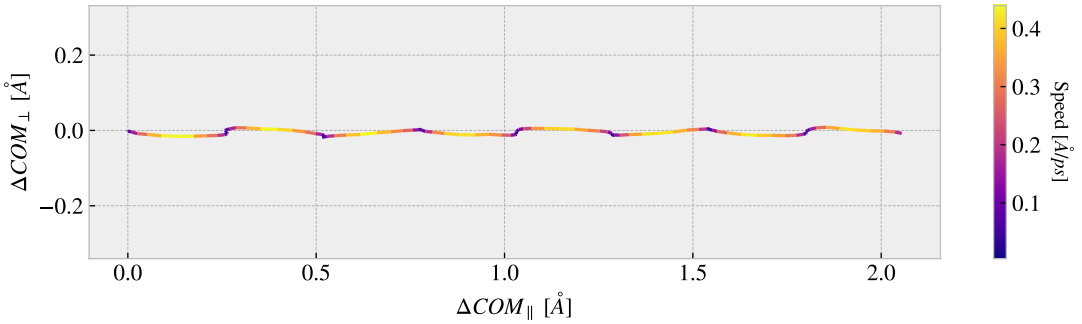

(a) $K = \inf$ (Fix move)

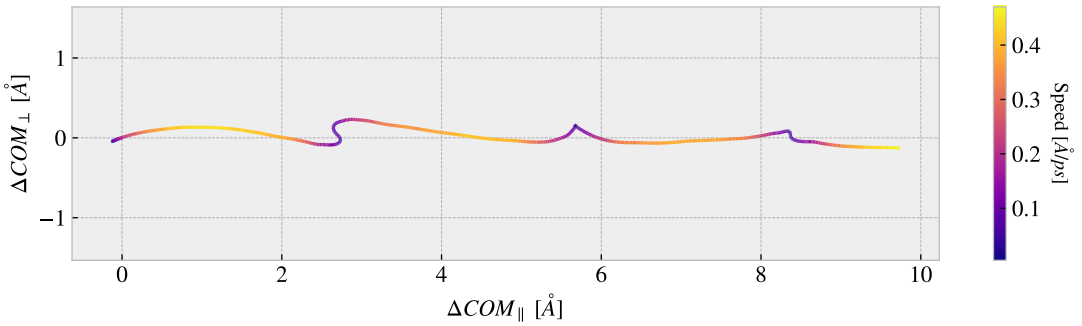

(b) 30 N/m

Figure 2.4: Center of mass posotion relative to the start of the sliding phase in terms of the direction parallel to the sliding direction $\Delta COM_\parallel$ and the axis perpendicular to the sliding direction $\Delta COM_\perp$. The colorbar denotes the absolute speed of the COM.

2.3 Defining metrics for dynamic and static friction

In order to evaluate the frictional properties of the sheet we aim to reduce the force trace results adressed in section Sec. 2.2 into single metrics describing the dynamic and static friciton.

2.3.1 Dynamic friction

For the dynamic friction measurement we take the mean value of the latter half of the dataset to ensure that we are sampling from a stable system. For a full sliding simulation of 400 Å we thus base our mean value on the latter 200 Å (1000 ps) of sliding. In Fig. 2.5a we have shown the force trace for the first 10 Å of sliding together with a 50% running mean window with the value being plotted at the end of the window. This is merely done to illustrate the samplig procedure, and we see that for such a short sliding period the final mean estimate (marked with a dot) takes a negative value due to the specific cut-off of the few oscialltion captured here. Nonetheless, one approach to quanity the uncertainy of the final mean estimate is to consider the variation of the running mean preceeding the final mean value. The more the running mean fluctuates the more uncertainty associated with the final estimate. However, only the running mean "close" to the ending should be considered, since the first part will rely on data from the beginning of the simulation. From the Fourier analyse in section Sec. 2.2.1 we found the longest significant oscillation period to be ~ 71 Å^{-1} corresponding to $\sim 35\%$ of the running mean window which have a window length of 200 Å when including all the data. Hence, we use the standard deviation of the final 35% of the running mean to approximate the uncertainty of the final mean value. We consider the standard deviation as an estimate of the absolute error and calculate the relative error by a division of the final mean value. In Fig. 2.5b we showcase a running relative error based on the standard deviation, with a window of length 35% the mena window, in a continuation of the illustrative case of a 10 Å sliding from Fig. 2.5a. In this case we get a high relative error of $\sim 257\%$ which alligns well with the short sampling period and the fact that this lead to the mean value taking an unphysical negative value.

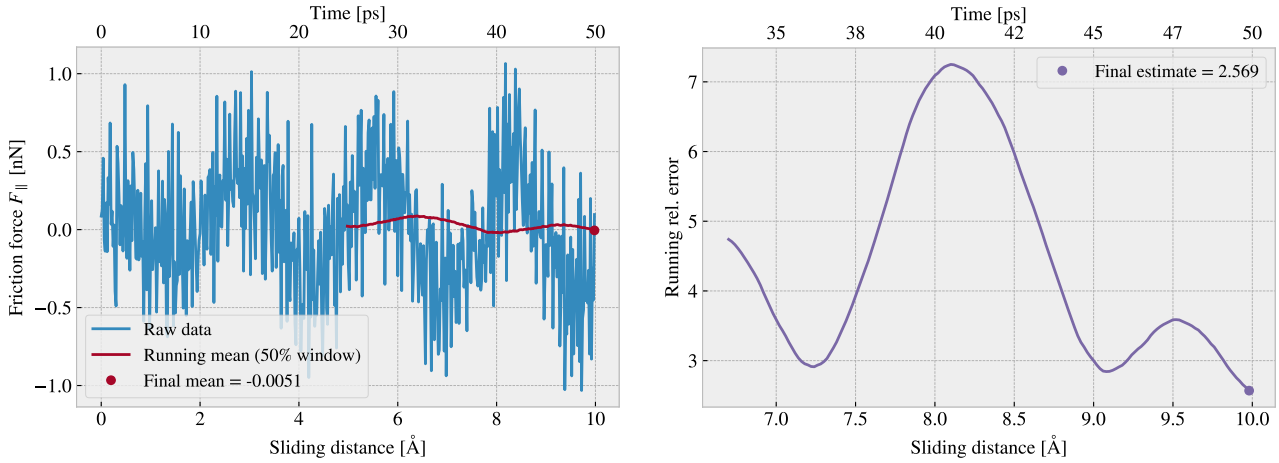

(a) Running mean with window length 5 Å (50% the data length).

(b) Running std with window length 1.75 Å (35% the mean window length.)

Figure 2.5: Running mean and running standard deviation (std) on the friction force data from a 10 Å of sliding simulation. The running mean window is 50% the data length while the running std window is 35% the running mean window length.

When including the full dataset of 400 Å of sliding, such that std window actually matches with the longest period of oscillations expected from the data, we get a final relative error of $\sim 12\%$ as shown in fig Fig. 2.6. This is arguable just at the limit for an acceptable error, but as we shall see later (Make a reference to fig or sec) this high relative error is mainly connected to the cases of low friction. When changing the simulation parameters, such that the mean friction evaluates to considerable higher values, the relative error drops to the order (put in numbers). One interpration of this finding is simply that the oscialltiosn in the running mean is somewhat independent of the magnitude of the friction. In that case, the relative error will spike for the low friction cases.

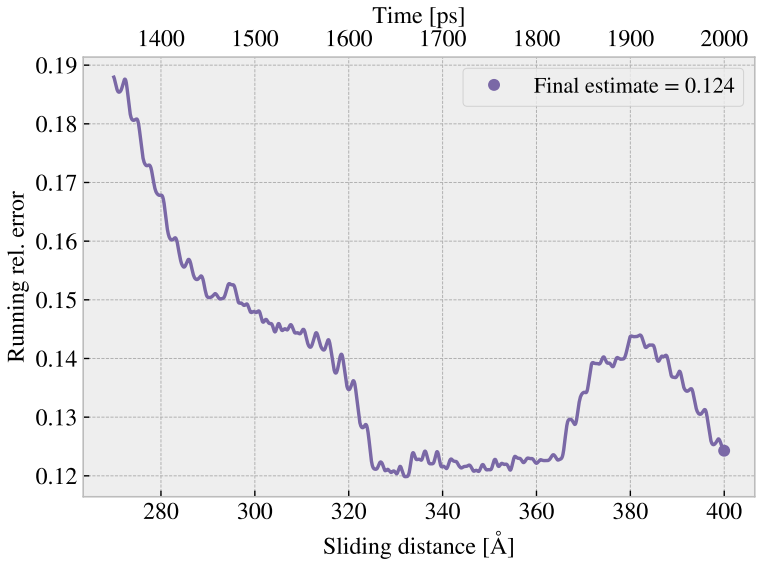

Figure 2.6: Running standard deviation (std) for a full 400 Å sliding simulation. The running std window is 70 Å (35% the running mean window of 50% the data length).

2.3.2 Static friction

The max value is the most obvious choice for adressing the static friction, even though that the definition of the static friction is a bit vague. When considering the friction force time series in Fig. 2.1 we observe that the

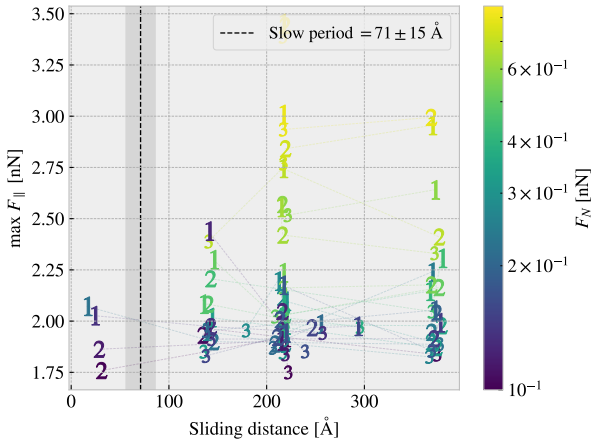

Figure 2.7: Distribution of top three max friction force peaks for 30 uniformly sampled normal forces $F_N \in [0.1, 10]$ nN. The dotted line and the grey area marks the slowest significant oscialltion period found in the data and thus marking a dividing line for whether a peak falls within the "beginning" of the sliding simulation.

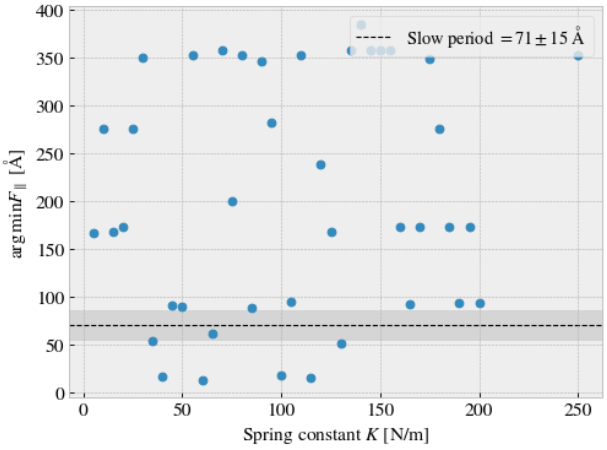

Figure 2.8: Sliding displacement for the max friction peak to appear as a function of spring constant. Fixmove is tmp mapped to K = 200 here without any discontinuous lines.

stick-slip oscillations increase in magnitude toward a global peak at ~ 20 Å. Thus, we could identify this peak as the static friction force, but the global max does in fact rarely fall within the first part of the sliding. In Fig. 2.7 we investigate the top three max value, at which sliding distance they accour and at what magnitude, for 30 uniformly sampled normal forces in the interval $[0.1, 10]$ nN. It is immediately clear that only few of the peaks falls within the "beginning" of the simulation defined by the slowest significant oscialltion period of 71 ± 15 Å. In fact only 2/30 global values and 4/90 top three values can be associated to the start of the sliding by this definition. Thus, this result suggest that the max value cannot be used as a reliable measure for the static friction either due to its lack of presence or due to the simulation setup procedure. For a more typycal evaluation of the static friction force one would increase force slowly until the first slip significant slip is recorded (a series of precursors is expected to precede this). In our simulations we drag the sheet relatively fast in a rigid manner which might be the reason for the lacking the static friction. Bonelli et al. [16] reported that the stick-slip behaviour was only presented when using a relatively soft spring. Thus, by changing the spring constant we investigate possibility to observe a static friction (I kind of interchanged stick-slip and static friction int his argument, but I still think it can be used to argue for doing the test...) response within the framework of our simulation procedure as shown in Fig. 2.8. However, the results do not indicate any implications that a recognizable domain exist for which the static friction response would be reliable. Hence, we will base the final assesment on frictional properties purely on the dynamic friction force.

2.3.3 Pressure reference for normal load domain

Find place to put this.

In order to relate the magntidue of the normal force in our friciton measurement we will use the pressure as a reference. We will use the pressure underneath a stiletto shoe as a worst case for human pressure execuation underneath the shoes. From (source 1) it is reported that the diameter of a stiletto heeled shoe can be less than 1 cm. Hence a 80 kg man[2] standing on one stiletto heel (with all the weight on the heel) will result in a pressure

$$P = \frac{F}{A} = \frac{mg}{r^2\pi} = \frac{80\,\text{kg} \cdot 9.8\,\frac{\text{m}}{\text{s}^2}}{(\frac{1 \times 10^{-2}\,\text{m}}{2})^2\pi} = 9.98\,\text{MPa}$$

[2]Yes, a man can certainly wear stilleto heels.

While this is in itself a spectacular realization that is often used in introductory physics courses (source 2) to demonstrate the rather extreme pressure under a stiletto heel (greater than the foot of an elephant) (how many Atmos?) this serves as a reasonible upperbound for human executed pressure. With a full sheet area of $\sim 21 \times 10^3\,\text{Å}^2$ we can achieve a similar pressure of $\sim 10\,\text{MPA}$ with a normal force of

$$F_N = 10\,\text{MPa} \cdot 21 \times 10^{-17}\,\text{m}^2 = 2.10\,\text{nN}$$

Of course this pressure might be insufficient for various industrial purposes, but with no specific procedure in mind this serves as a decent reference point. Notice that if we consider a human foot with ares $113\,\text{cm}^2$ the pressure drops to a mere $70\,\text{kPa}$ corresponding to $\sim 0.01\,\text{nN}$.

2.4 Out of plane buckling

The out of plane buckling is the main motivation for applying the kirigami inspired cuts to the sheet. Thus, we perform a stretch simulation in a low temperature $T = 5\,\text{K}$ vacuum in order to verify that the chosen cut configurations do in fact contribute to a significant out of plane buckling when stretched. For the non-cut, popup and honeycomb configuration we assess the movement in the z-direction (perpendicular to the plane) during the stretch, which we visualize by the min and max z-value along with the atom count quartiles 1%, 10%, 25%, 50% (median), 75%, 90% and 99% as shown in figure Fig. 2.9. We observe that the popup and honeycomb pattern buckles considerable out of plane during the stretch in comparison to the non-cut sheet which only exhibit minor buckling of ~ 2 Å which is on the same order as the atomic spacing in the sheet. We also notice that the popup pattern buckles more in consideration to the min and max peaks while the 1%, 99% quartiles is on the same magnitude as the honeycomb. By looking at the simulation visualization (include OVITO figures for vacuum stretch as well?) we can conclude that this is mainly due to the fringes of the sheet "flapping" around.

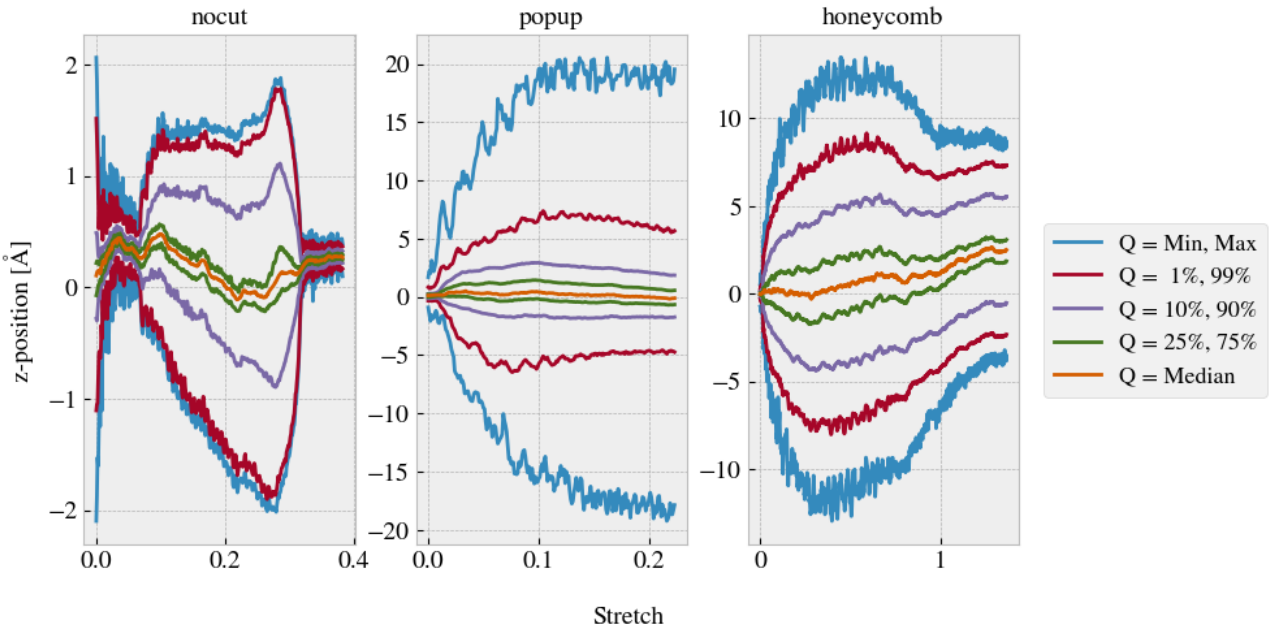

Figure 2.9: Out of plane buckling during stretch of sheets in vacuum at $T = 5$ K. Reading from left to right the vacuum rupture stretch are 0.38, 0.22 and 1.37. perhaps use a color scale instead of the standard color cycles here.

The next step is to verify that the buckling will lead to a significant altering of the contact area when the sheet is in put in contact with the substrate. We investigate this by simulating the stretch at the default temperature $T = 300\,\text{K}$ with the presence of contact forces between the sheet and substrate. Note that no normal load is applied as the sheet and substrate is sufficiently attracted by the LJ potential. Selected frames from the simulation is shown in appendix **??**. We assess the contact area by the relative amount of atoms in the sheet within chemical range of the substrate. The cut-off for this interaction is 4 Å corresponding to $\sim 120\%$

the LJ equilibrium distance. Since the contact area is usually calculated as the amount of atoms in contact multiplied with an associated area for each contact this feature is taken to be proportional to the contact area. The relative amount of bonds as a function of stretch for the various configurations is shown in figure Fig. 2.10 which clearly indicates a drop in contact area as the cutted sheets are stretched.

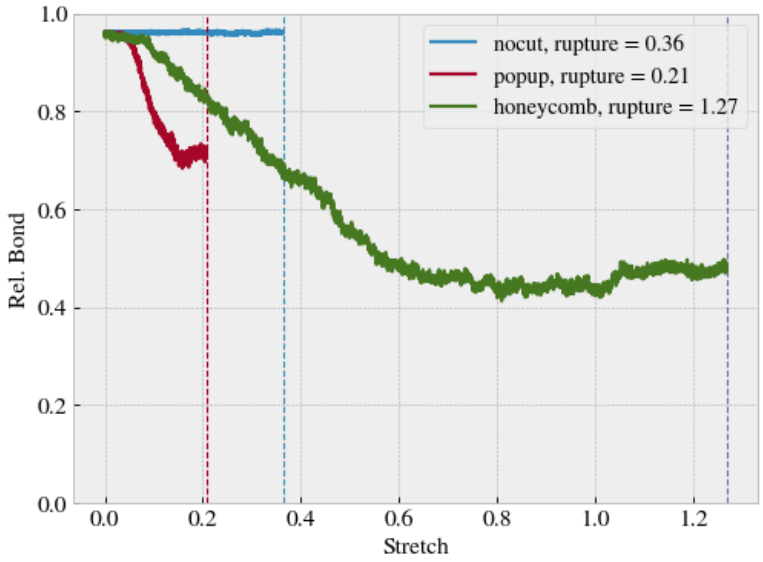

Figure 2.10: Contact vs. stretching of the sheet, where the contact is measured by the relative amount atoms in the sheet within chemical interaction range to the substrate. The cut-off for this interaction range is 4 Å corresponding to $\sim 120\%$ the LJ equilibrium distance. $T = 300$ K

Compare figure Fig. 2.10 to that of figure Fig. 2.15 where multiple simulations constitute the stretch-contact curve.

2.5 Investigating selected parmeters

We investigate the importance of the physical variables T, v_{slide} and K (make plots for scan angle as well?) and the choice of timestep dt. This is done partly understand how the dependencies relate to theoretical, numerical and experimerimental results, and partly to understand how these parameter choices defines the regime for our multi configurational search. We use the default parameters in **??** with exception of the single parameter of interest which is varied in a reasonable range of the default choice. In Fig. 2.11-Fig. 2.14 the dynamic friction estimate and the max friction force is shown as a function of T, v_{slide}, K and dt respectively. For the dynamic friction estimate the absolute error is denoted by a shaded error which linearly connects the points.

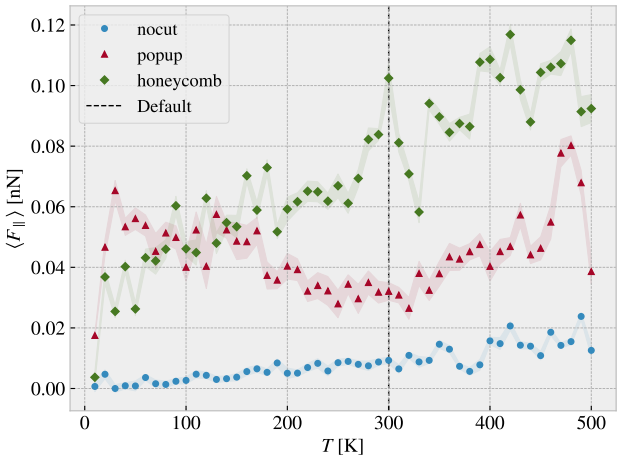

(a) Dynamic friction force estimate.

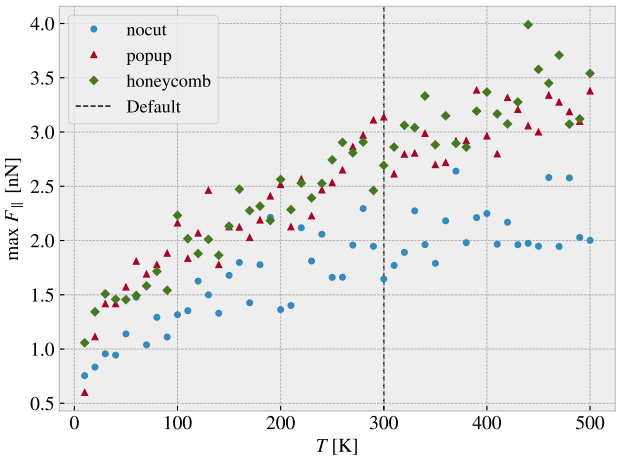

(b) Max friction

Figure 2.11: Temperature.

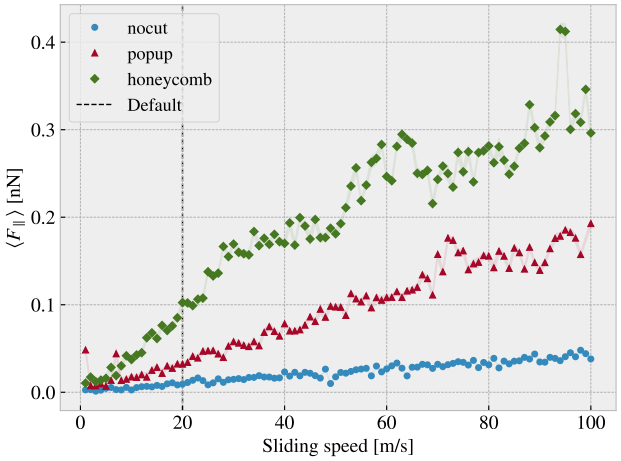

(a) Dynamic friction force estimate.

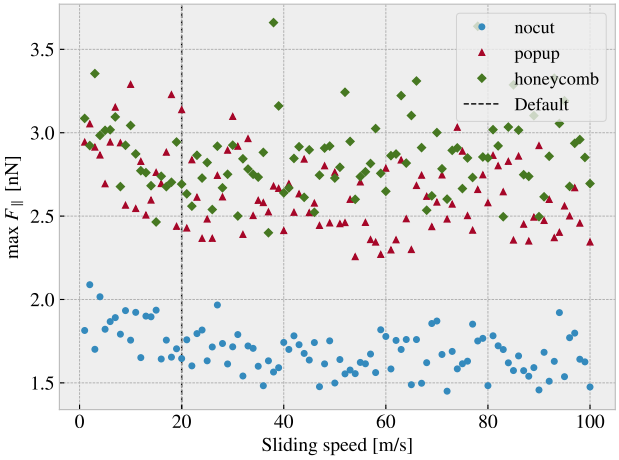

(b) Max friction

Figure 2.12: Sliding speed

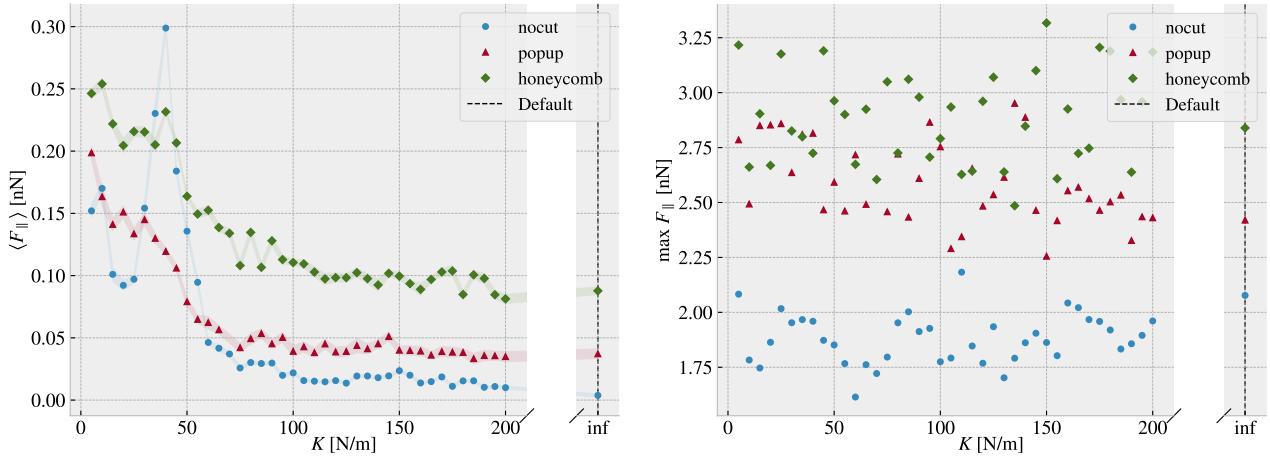

(a) Dynamic friction force estimate. **(b)** Max friction

Figure 2.13: Spring constant

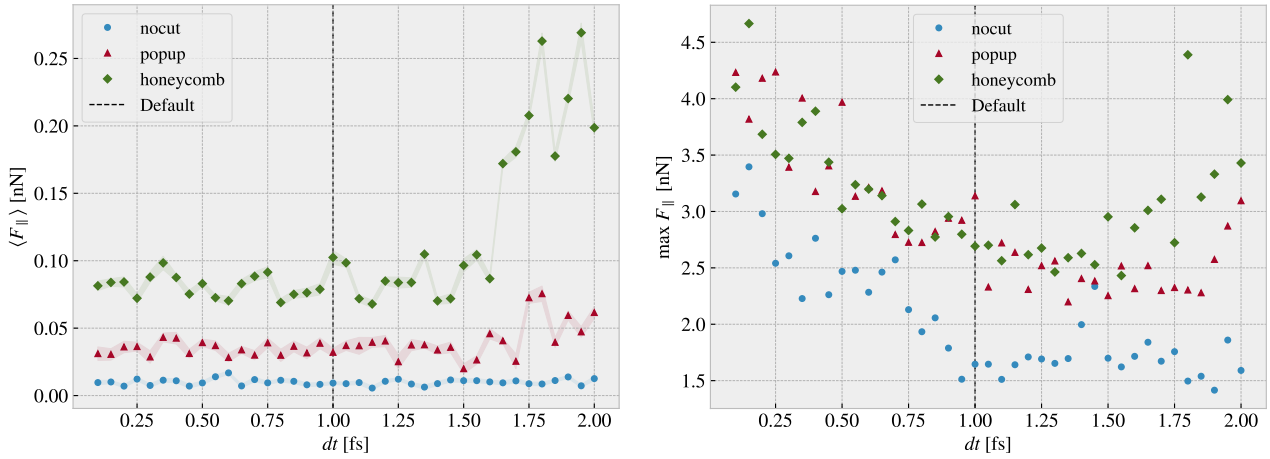

(a) Dynamic friction force estimate. **(b)** Max friction

Figure 2.14: Timestep

Quick thoughts:

- Temperature: We do clearly not see the $1/T$ temperature decrease. The non-cut sheet seems to showcase a lienar relationship which is also somewaht present for the honeycomb which matches some of the findings in other MD simulations. For the popup we do see a local decrease at low temperatures which flip at around the default $T = 300\,\mathrm{K}$ temperature. The max friction peaks seem to increase with temperatur as well indicating that the peaks might be associated with thermal fluctuations rather than actual stick-slip behaviour. This supports the finding that the static friction response is not significantly present in these simulations.

- Velcotiy: Considering the non-cut sheet first the velocity dependency is seemingly linear which deviates from the expected logaritmic trend. For the cutted configurations we find some peaks which might indicate the presence of resonance frequencies. The cutted sheet might be closer to a logaritmic trend, but this is not spot on either. The max friction seems to decrease slightly with small velcoties and then stay rather constant. This can probably be explained by the reduced time to stick between stick slip.

- Spring constant: On all three configurations the dynamic friction decreases with an increasing spring constant. The best explanations might be due to the lack of freedom to "get stuck" in incommensurable

configurations. We also notice that the friction varies a lot at lower spring constants supporting the choice of having a stiff spring for stability reasons. Especially the non-cut sheet peaks at $K = 40\,\mathrm{N/m}$. The max friction seem to be constant with K.

- dt: The dynamic friction is relatively stable around the default choice of $dt = 1\,\mathrm{fs}$. However, the fluctuations with respect to dt is more significant for popup pattern and even more for the honeycomb pattern. This indicates that the more complex dynamics of the simulation is more sensitive to the timestep. We might interpret this information as an additional measure of uncertainty. The maximum friction decreases with increasing timestep which can be asserted a statistical interpretation: Higher peaks will be captured by the high resolution of a low dt and vice versa. The high max values towards the point of $dt = 2\,\mathrm{fs}$ is most likely due to the approach of unstability in the simulation as seen more clearly for the dynamic friction evaluation.

2.6 Normal force and stretch dependencies

Till this point we have only changed variables one by one to investigate single dependencies. We now advance the sutdy to a simultaneous variation of stretch and normal force.

Explain how the stretch is uniformly sampled within equally divided intervals and the normal force is actually uniformly sampled in a given range. Argue that the first might be approximately uniformly distributed for large numbers.

Talk about rupture test also. Maybe in the theory/method section under numerical procedure: Before simulating a rupture test is perform to determine under what stretch the sheet ruptures. This is a slightly higher threshold than when applied normal load and sliding along the substrate.

2.6.1 Contact area

??

We reproduce the contact area investigation of Fig. 2.10 with the modificaiton that the contact count is measured as an average of the latter 50% of the sliding simulation at a non-zero applied normal load. The results are shown in Fig. 2.15 with 30 attempted (some rupture) stretch (pseudo) uniformly distributed stretch between 0 and the rupture point and 3 uniform distributed normal loads in the interval $[0.1, 10]$ nN.

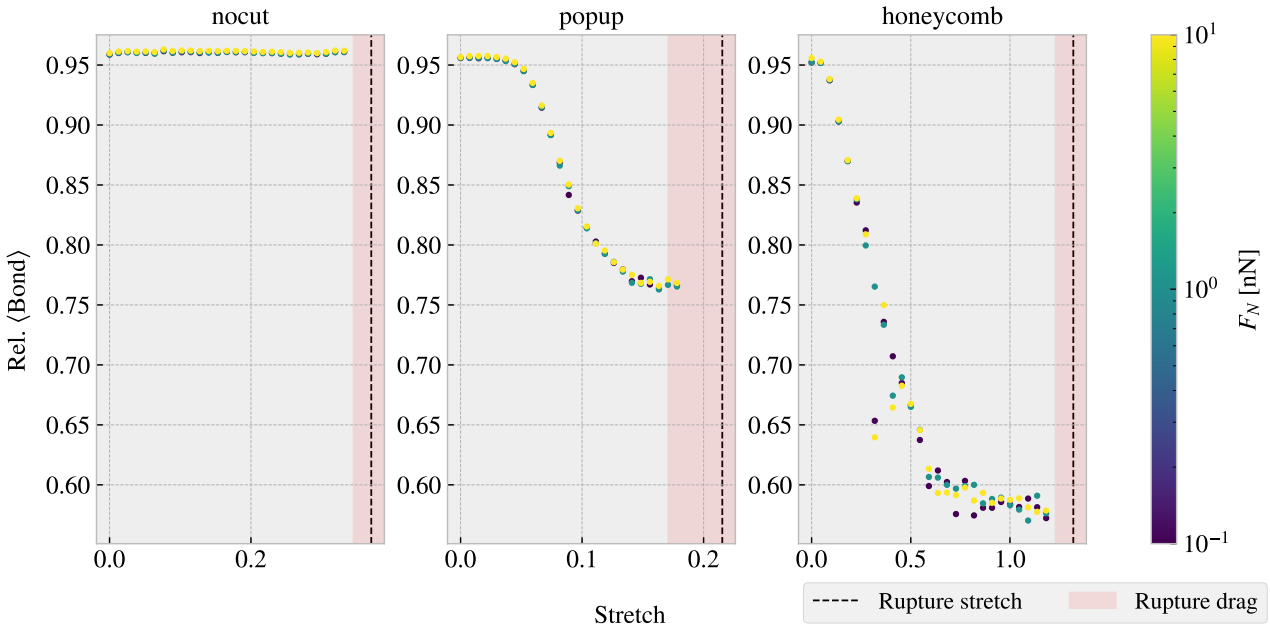

Figure 2.15: Average relative amount of bonds beetwen the sheet and the substrate defined by the cut-off distance of 4 Å. The average is taken over the latter half of the sliding phase. The red shade denotes the stretch range where ruptures accour at certain normal loads under sliding while the black-dotted line represent the rupture point due to stretching (rupture test)

From Fig. 2.10 we observe a significant decrease in the contact due to stretching of the cut configurations in contrast to the non-cut which stays roughly constant. This is reminiscent of the non-sliding stretch vs. contact curve shown in Fig. 2.10. Given these results, theoretically one would expect the dynamic friction to decrease with stretch for the cut configurations.

2.6.2 Stretch

We make a similar analysis as done in the previous section **??** with the substitution of friction force instead of contact (The data is taken from the same simulaitons runs). The dynamic friction force (put uncertainty here even though that it is quite low?) and the max friction is shown in Fig. 2.16a and Fig. 2.16 respectively.

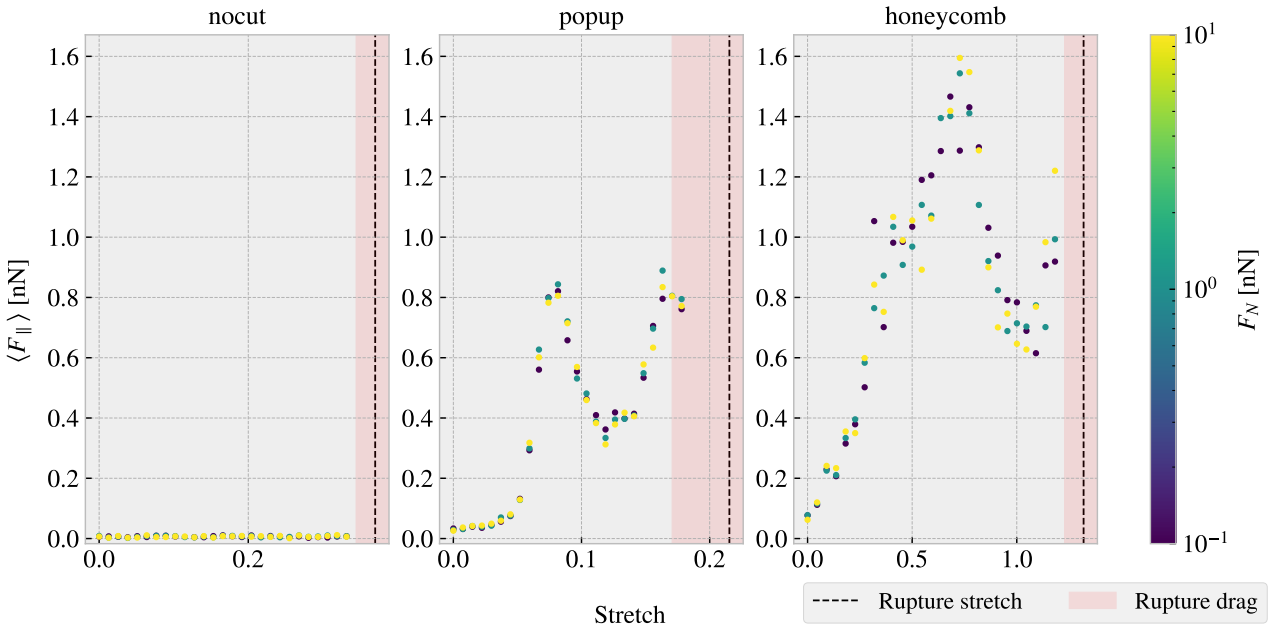

(a) Dynamic friction estimate.

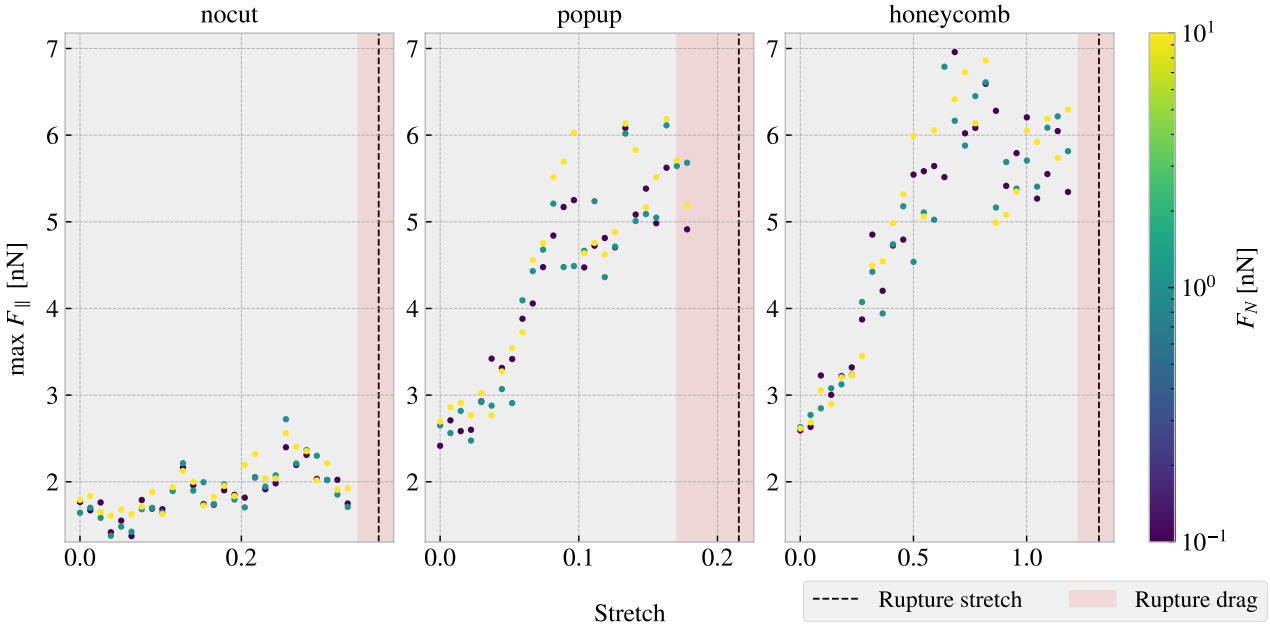

(b) Max friction

Figure 2.16: CAPTION

From Fig. 2.16a we find to our surprise that the dynamic friction increase with stretch for the cut configurations despite a simmutaneous decrease in contact area as shown in figure Fig. 2.15. This suggests that the amount of chemical bonding atoms is not the dominant mechanism for the friction of this system. Instead, we might point to a mechanism more mechanical of nature associated to phonon exications. When the cut sheet is strecthed the stress (show stress maps somewhere or not nessecary?) might induce a certain distribution and magnitude of point pressures to favor energy dissipation. Nonetheless, the results showcase a strong coupling between stretch and friction force, also for the max friction force, which is beyond the expectations at this stage of the study. The non-cut configuration does not show significant dependency on the stretch which reveal that this effect is only present when combining cut and stretch and not purely by strecthing the sheet.

By considering the increase in dynamic friction towards the first peak we get a relative friction increase and increase vs. stretch ratios as described in Table 2.2. While the honeycomb force increase towards the first peak is approximately linear the popup exhibits seemingly exponential growth which yield a slope on the order $\sim 30\,\text{nN}$.

Table 2.2: (stretch, dynamic friction) coordinates from Fig. 2.16a at start and the first peak respectively used to approximate the relative increase in friction force and the ratio for friction increaese vs. stretch for sait range. In practice the latter ratio denotes the slope of a forced linear trend.

Configuration	Start	First peak	Relative increase	Friction force vs. stretch ratio [nN]
Popup	$\sim (0, 0.03)$	$\sim (0.082, 0.83)$	27.7	9.76
Honeycomb	$\sim (0, 0.07)$	$\sim (0.728, 1.57)$	22.4	2.06

Additionally, we notice that booth the popup and honeycomb also exhibits stretch ranges where the dynamic friction force decrease with increasing stretch. Qualitatively we assign the slope to be on the same order of magnitude as those towrds the first peak. This is useful for the prospect of taking advantage of this phenonama as we can essentially achieve booth higher and lower friction for increasing stretch for different starting points.

2.6.3 Normal force

Main take away from this section should be that the normal force does not really change the friction much; The friciton coefficient is extremely low, but I'm not sure how well the linear fits are (whether they are linear or sublinear). Not sure if I should do a linearly increasing normal force for better linear plots?

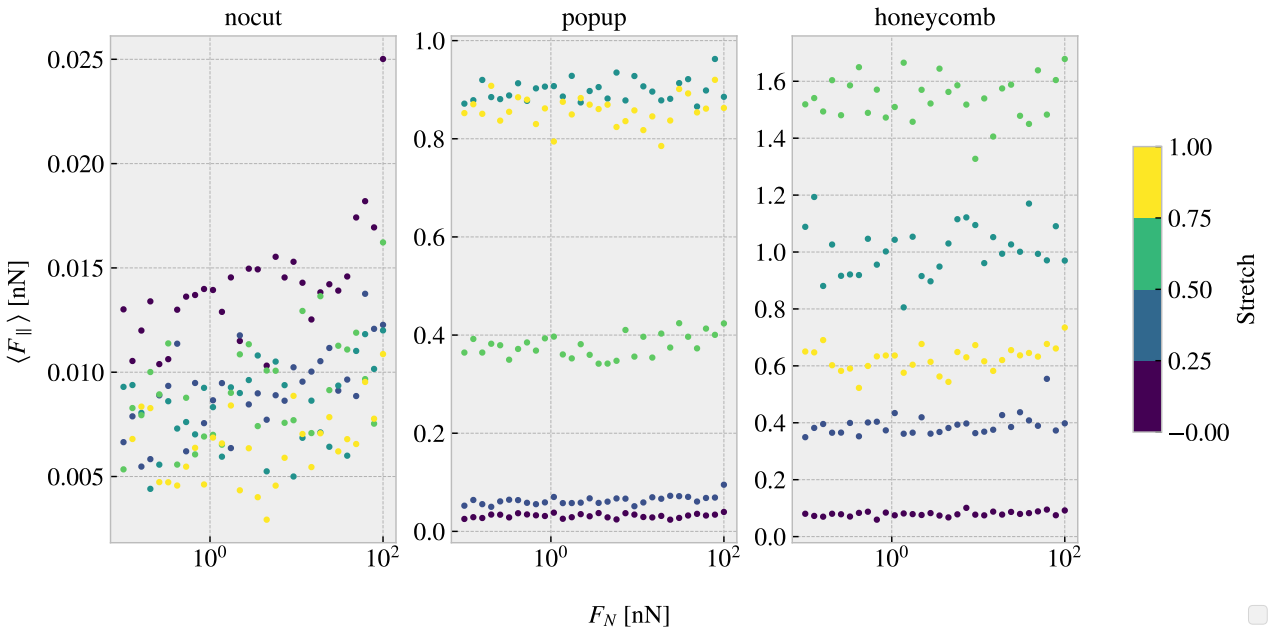

Figure 2.17: ...

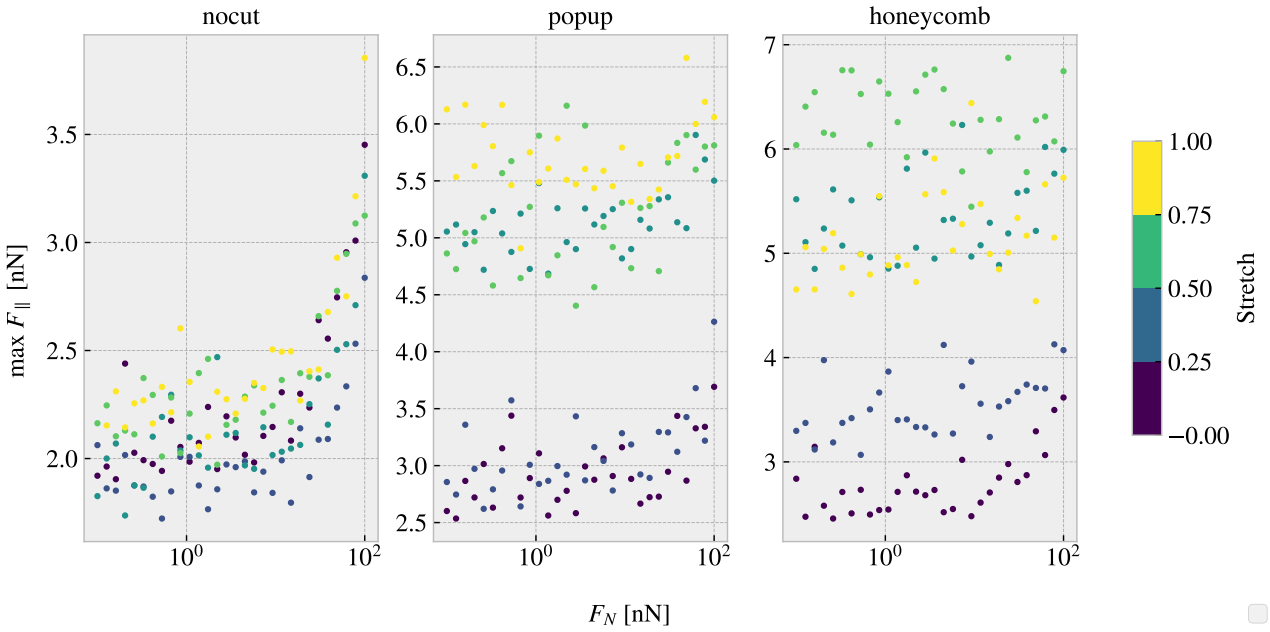

Figure 2.18: Colorbar is only fitted for the right plot (honeycomb)... this should be fixed. Should I have run a linear distribtion of FN so I could plot it linear here also...?

Table 2.3: Mean friction coeff

nocut	$0.00009 \pm 1 \times 10^{-5}$	$0.00005 \pm 1 \times 10^{-5}$	$0.00004 \pm 1 \times 10^{-5}$	$0.00005 \pm 2 \times 10^{-5}$	
popup	$0.00005 \pm 3 \times 10^{-5}$	$0.00024 \pm 5 \times 10^{-5}$	$0.0002 \pm 2 \times 10^{-4}$	$0.0005 \pm 1 \times 10^{-4}$	$0.0003 \pm 2 \times 10^{-4}$
honeycomb	$0.00013 \pm 6 \times 10^{-5}$	$0.0006 \pm 3 \times 10^{-4}$	$0.0004 \pm 6 \times 10^{-4}$	$0.0007 \pm 6 \times 10^{-4}$	$0.0009 \pm 3 \times 10^{-4}$

Table 2.4: Max friciton coeff

nocut	$0.0139 \pm 9 \times 10^{-4}$	$0.0083 \pm 7 \times 10^{-4}$	$0.010 \pm 1 \times 10^{-3}$	$0.0105 \pm 9 \times 10^{-4}$	
popup	$0.007 \pm 2 \times 10^{-3}$	$0.010 \pm 2 \times 10^{-3}$	$0.007 \pm 2 \times 10^{-3}$	$0.009 \pm 3 \times 10^{-3}$	$0.006 \pm 2 \times 10^{-3}$
honeycomb	$0.010 \pm 1 \times 10^{-3}$	$0.007 \pm 2 \times 10^{-3}$	$0.007 \pm 3 \times 10^{-3}$	$0.000 \pm 3 \times 10^{-3}$	$0.004 \pm 3 \times 10^{-3}$

One theory for the low friction coefficient might dependent on the fact that the normal force is only applied on the pull blocks. Especially with the cutted sheet the tension drops such that the effecive normal force on the inner sheet is not changing very much. By this theory the friction force vs. normal force on the pull blocks should look a bit more like expected and we might make some plots of thoose to check

When looking at the graphs for the PB the max friction is visually textbook linear, while the mean friction is a bit more linear but also with negativ coefficients...

2.7 Computational cost

Talk about the computatonal cost of different choices. How does computation time scale with drag speed, dt and maybe T and K as well. One could also mention scaling with system size.

Show how the number of cores per simulation scale to argue that running on just one core (maybe 4) is smart for the next step of many simulations.

Mention the trouble with GPU to show that this was considered, and in fact this was the reason for choosing the Tersoff potential over the AIREBO which is perhaps more common these days...

Appendices

Appendix A

Appendix B

Appendix C

Bibliography

[1]E. Gnecco and E. Meyer, *Elements of friction theory and nanotribology* (Cambridge University Press, 2015).

[2]Bhusnan, "Introduction", in *Introduction to tribology* (John Wiley & Sons, Ltd, 2013) Chap. 1, 1–?

[3]H.-J. Kim and D.-E. Kim, "Nano-scale friction: a review", International Journal of Precision Engineering and Manufacturing **10**, 141–151 (2009).

[4]K. Holmberg and A. Erdemir, "Influence of tribology on global energy consumption, costs and emissions", Friction **5**, 263–284 (2017).

[5]B. Bhushan, "Gecko feet: natural hairy attachment systems for smart adhesion – mechanism, modeling and development of bio-inspired materials", in *Nanotribology and nanomechanics: an introduction* (Springer Berlin Heidelberg, Berlin, Heidelberg, 2008), pp. 1073–1134.

[6]P. Z. Hanakata, E. D. Cubuk, D. K. Campbell, and H. S. Park, "Accelerated search and design of stretchable graphene kirigami using machine learning", Phys. Rev. Lett. **121**, 255304 (2018).

[7]P. Z. Hanakata, E. D. Cubuk, D. K. Campbell, and H. S. Park, "Forward and inverse design of kirigami via supervised autoencoder", Phys. Rev. Res. **2**, 042006 (2020).

[8]L.-K. Wan, Y.-X. Xue, J.-W. Jiang, and H. S. Park, "Machine learning accelerated search of the strongest graphene/h-bn interface with designed fracture properties", Journal of Applied Physics **133**, 024302 (2023).

[9]Y. Mao, Q. He, and X. Zhao, "Designing complex architectured materials with generative adversarial networks", Science Advances **6**, eaaz4169 (2020).

[10]Z. Yang, C.-H. Yu, and M. J. Buehler, "Deep learning model to predict complex stress and strain fields in hierarchical composites", Science Advances **7**, eabd7416 (2021).

[11]A. E. Forte, P. Z. Hanakata, L. Jin, E. Zari, A. Zareei, M. C. Fernandes, L. Sumner, J. Alvarez, and K. Bertoldi, "Inverse design of inflatable soft membranes through machine learning", Advanced Functional Materials **32**, 2111610 (2022).

[12]S. Chen, J. Chen, X. Zhang, Z.-Y. Li, and J. Li, "Kirigami/origami: unfolding the new regime of advanced 3D microfabrication/nanofabrication with "folding"", Light: Science & Applications **9**, 75 (2020).

[13]Z. Deng, A. Smolyanitsky, Q. Li, X.-Q. Feng, and R. J. Cannara, "Adhesion-dependent negative friction coefficient on chemically modified graphite at the nanoscale", Nature Materials **11**, 1032–1037 (2012).

[14]R. W. Liefferink, B. Weber, C. Coulais, and D. Bonn, "Geometric control of sliding friction", Extreme Mechanics Letters **49**, 101475 (2021).

[15]P. Zhu and R. Li, "Study of nanoscale friction behaviors of graphene on gold substrates using molecular dynamics", Nanoscale Research Letters **13**, 34 (2018).

[16]F. Bonelli, N. Manini, E. Cadelano, and L. Colombo, "Atomistic simulations of the sliding friction of graphene flakes", The European Physical Journal B **70**, 449–459 (2009).